STRUCTURAL BIOLOGY COMMUNICATIONS

ISSN 2053-230X

# Changes in the allosteric site of human liver pyruvate kinase upon activator binding include the breakage of an intersubunit cation–$\pi$ bond

Jeffrey S. McFarlane,[a] Trey A. Ronnebaum,[b] Kathleen M. Meneely,[a] Annemarie Chilton,[a] Aron W. Fenton[c]* and Audrey L. Lamb[a,b]*

[a]Department of Molecular Biosciences, University of Kansas, 1200 Sunnyside, Lawrence, KS 66045, USA, [b]Department of Chemistry, University of Kansas, 1200 Sunnyside, Lawrence, KS 66045, USA, and [c]Department of Biochemistry and Molecular Biology, University of Kansas Medical Center, 3901 Rainbow Boulevard, Kansas City, KS 66160, USA. *Correspondence e-mail: afenton@kumc.edu, lamb@ku.edu

Received 29 January 2019
Accepted 18 May 2019

Edited by R. J. Read, University of Cambridge, England

**Keywords:** pyruvate kinase; allosterism; human liver isozyme.

**PDB references:** human liver pyruvate kinase, D499N variant, 6nn4; W527H variant, 6nn5; Δ529/S531G variant, 6nn7; S531E variant, 6nn8

**Supporting information:** this article has supporting information at journals.iucr.org/f

Human liver pyruvate kinase (hLPYK) converts phosphoenolpyruvate to pyruvate in the final step of glycolysis. hLPYK is allosterically activated by fructose-1,6-bisphosphate (Fru-1,6-BP). The allosteric site, as defined by previous structural studies, is located in domain C between the phosphate-binding loop (residues 444–449) and the allosteric loop (residues 527–533). In this study, the X-ray crystal structures of four hLPYK variants were solved to make structural correlations with existing functional data. The variants are D499N, W527H, Δ529/S531G (called GGG here) and S531E. The results revealed a conformational toggle between the open and closed positions of the allosteric loop. In the absence of Fru-1,6-BP the open position is stabilized, in part, by a cation–$\pi$ bond between Trp527 and Arg538′ (from an adjacent monomer). In the S531E variant glutamate binds in place of the 6′-phosphate of Fru-1,6-BP in the allosteric site, leading to partial allosteric activation. Finally, the structure of the D499N mutant does not provide structural evidence for the previously observed allosteric activation of the D499N variant.

## 1. Introduction

Human liver pyruvate kinase (hLPYK) catalyzes the conversion of phosphoenolpyruvate (PEP) to pyruvate through a phosphoryl transfer from PEP to ADP, generating pyruvate and ATP. In human liver, this penultimate step of glycolysis is allosterically regulated by fructose-1,6-bisphosphate (Fru-1,6-BP), an earlier intermediate of glycolysis. Like many other allosteric systems, the structural changes that constitute the allosteric mechanism and give rise to altered function (*i.e.* a change in ligand affinity or catalysis; Carlson & Fenton, 2016) are not well defined for hLPYK.

The binding position of Fru-1,6-BP in the allosteric site of pyruvate kinase (PYK) was first identified in yeast PYK (Jurica *et al.*, 1998) and later in human erythrocyte PYK (Valentini *et al.*, 2002). Previously, two hLPYK structures have been solved (PDB entries 4ima and 4ip7), both with Fru-1,6-BP bound in the allosteric site (Holyoak *et al.*, 2013). In a subsequent study (Ishwar *et al.*, 2015), binding and allosteric activation were assayed for a Fru-1,6-BP effector-analog series and a mutational series that targeted residues surrounding the allosteric site, including D499N, W527H, Δ529/S531G (GGG) and S531E (Fig. 1). Analysis of these data led to several hypotheses. (i) Asp499 regulates allosteric coupling across a tetramerization interface between the adjacent C-domain subunits (the C–C interface), possibly through interactions with Trp527 or Arg528 of the allosteric loop (residues

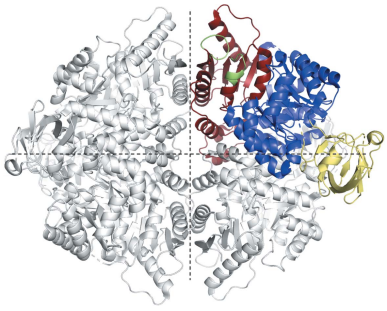

527–533) when Fru-1,6-BP is absent. (ii) The increase in PEP affinity observed for the D499N and W527H mutants in the absence of Fru-1,6-BP is due to the disruption of allosteric coupling across the C–C interface. (iii) The 6′-phosphate of Fru-1,6-BP contributes to binding by interacting with the phosphate-binding loop (residues 444–449 between $\beta$1 of sheet D and $\alpha$22). A glutamate mutation of the allosteric loop serine (S531E) was found to mimic allosteric activation (*i.e.* increase PEP affinity) in the absence of Fru-1,6-BP (Ishwar *et al.*, 2015). It was proposed that this gain of function was due to the S531E glutamate binding to the 444–449 loop in place of the 6′-phosphate of Fru-1,6-BP.

In this study, we examine the structural basis for the above hypotheses derived from the previously published allosteric activity data (Ishwar *et al.*, 2015) by solving four X-ray crystal structures of hLPYK variants: D499N, W527H, S531E and GGG (deletion of Pro529 and an S531G substitution, resulting in a glycine in each position from 530 to 532). This focus allows a direct comparison of different conformations of the allosteric site in a single PYK isozyme and offers a contrast to past studies that compared the structures of different isozymes, including human muscle pyruvate kinase $M_2$PYK and $M_1$PYK (Dombrauckas *et al.*, 2005; Morgan *et al.*, 2013). Our functional characterizations show that the D499N and W527H mutants both serve to mimic allosteric activation by Fru-1,6-BP and were included in this structural analysis to evaluate the previously proposed interaction between Asp499 and Tyr527′ or Arg528′ (the prime symbol is used to designate a residue from an adjacent monomer). In contrast, the GGG variant demonstrated a lack of functional response to Fru-1,6-BP, and was generated for this structural study to test the effect of a shortened, more flexible allosteric loop with a reduced propensity to make hydrogen bonds to bound Fru-1,6-BP. The S531E mutation mimics Fru-1,6-BP activation in functional assays. Here, the S531E variant structure was solved to test the hypothesis that glutamate, substituted at position 531, is able to bind within the allosteric site in place of Fru-1,6-BP, leading to partial activation. The results from this structural study build on the previous functional characterizations of mutants to reveal conformational changes that occur in the allosteric loop in the presence and absence of Fru-1,6-BP, confirm the proposed position of glutamate in the S531E variant and cause a revision of the proposed hypothesis regarding Asp499. The presence of a cation–$\pi$ interaction between Trp527 and Arg538′ across the C–C interface was observed, but an interaction between Asp499′ and Trp527 or Arg528 was not.

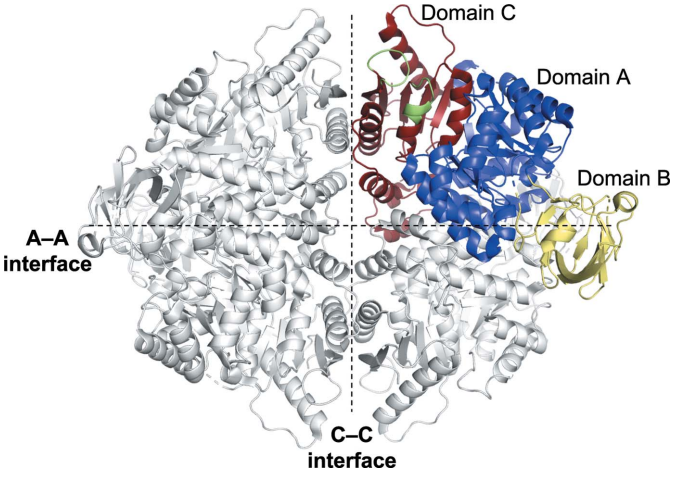


**Figure 1**
Structural overview of hLPYK. Model of hLPYK (PDB entry 4ip7). Each monomer of the homotetramer is composed of three domains (A, B and C). The B domain interacts with the A domain of the same subunit. The A–A interface is formed between A domains from adjacent monomers. The C–C interface is formed by adjacent C domains. The allosteric sites are positioned along the C–C interface (shown in green for one monomer).

## 2. Methods

### 2.1. Preparation of overexpression plasmids

The wild-type human liver *pyk* gene (UniProt ID P30613) was codon-optimized for expression in *Escherichia coli* and purchased from GenScript in a pUC57 vector with a 5′ NdeI restriction site and a 3′ XhoI restriction site. The gene was digested and inserted into a p15TV-L vector (Addgene plasmid 26093) using the restriction enzymes NdeI and XhoI. The resultant plasmid encodes the wild-type human liver *pyk* gene with an N-terminal hexahistidine tag that can be cleaved with TEV protease. The hLPYK variants were produced by QuikChange mutagenesis (Agilent) using the wild-type hLPYK plasmid as the template with forward primers 5′-GTTACC GGTTGGCGTCCGGGTGAAGGCTATACCAACATC for the S531E variant, 5′-GATCTGGGCGGACGATGTTAACC GTCGTGTG for the D499N variant, 5′-GGTTACCGGTTG GCGTGGTGGCGGCTATA for the GGG variant and 5′-TG GTGATCGTGGTTACCGGTCACCGTCCGGGTAGC for the W527H variant and the complementary reverse primers. The variant plasmids were sequenced by ACGT Inc. and contained only the desired mutation. All plasmids were transformed into *E. coli* BL21 Star (DE3) cells (Invitrogen) for protein overexpression.

### 2.2. Protein overexpression and purification

*E. coli* BL21 Star (DE3) cells containing the expression plasmid for the hLPYK variants were grown in LB medium containing 200 µg ml$^{-1}$ ampicillin at 37°C with shaking (225 rev min$^{-1}$) until an $OD_{600}$ of ∼1.0 was reached. The cultures were induced with 0.2 m*M* isopropyl $\beta$-D-1-thiogalactopyranoside and the temperature was reduced to 15°C for 20 h. The cells were harvested by centrifugation (6000*g*, 10 min, 4°C). The cell pellet was resuspended in 15 ml 50 m*M* Tris–HCl pH 8.5, 500 m*M* NaCl, 50 m*M* imidazole, 10 m*M* KCl, 5 m*M* $MgCl_2$ (buffer *A*) per litre of culture. The cells were disrupted using a French pressure cell (241 MPa) and cellular debris was removed by centrifugation (12 000*g*, 30 min, 4°C). The supernatant was applied onto a Chelating Sepharose Fast-Flow column (Amersham Biosciences) charged with nickel chloride and pre-equilibrated in buffer *A*. hLPYK eluted at ∼150 m*M* imidazole in a linear gradient of 50–500 m*M* imidazole in buffer *A*. The pooled fractions

**Table 1**
Crystallization.

| Variant | D499N | W527H | GGG | S531E |
|---|---|---|---|---|
| Method | All crystals were grown by hanging-drop vapor diffusion at 298 K in VDX 24-well plates | | | |
| Protein concentration (mg ml$^{-1}$) | 3.6 | 6.0 | 2.0 | 2.0 |
| Buffer composition of protein solution | 50 m*M* MES pH 6.8, 100 m*M* KCl, 10% glycerol, 2 m*M* DTT | 50 m*M* MES pH 6.8, 100 m*M* KCl, 10% glycerol, 2 m*M* DTT | 50 m*M* MES pH 6.8, 100 m*M* KCl, 10% glycerol, 2 m*M* DTT | 50 m*M* MES pH 6.8, 100 m*M* KCl, 10% glycerol, 2 m*M* DTT |
| Composition of reservoir solution | 200 m*M* ammonium citrate dibasic, 20% PEG 3350 | 325 m*M* ammonium citrate dibasic, 16% PEG 3350 | 200 m*M* ammonium citrate pH 6.0, 24% PEG 3350 | 200 m*M* ammonium citrate pH 5.6, 16% PEG 3350 |
| Volume and ratio of drop | 3.0 µl, 1:1 | 3.0 µl, 1:1 | 3.0 µl, 1:1 | 3.0 µl, 1:1 |
| Volume of reservoir (µl) | 1000 | 1000 | 1000 | 1000 |

were applied onto a Superdex 200 size-exclusion column (GE Life Sciences) equilibrated with 50 m*M* 2-(*N*-morpholino)ethanesulfonic acid (MES) pH 6.8, 100 m*M* KCl, 10% glycerol. The fractions containing hLPYK were pooled and dithiothreitol (DTT) was added to a final concentration of 2 m*M*; the pooled fractions were concentrated using an Amicon stirred cell with a YM-30 membrane to ∼5 mg ml$^{-1}$ as determined by the Bradford assay and were stored at −80°C.

### 2.3. Protein crystallization

All proteins were crystallized with their N-terminal hexahistidine tag intact. All crystals were grown in hanging drops composed of 1.5 µl protein solution and 1.5 µl well solution (described below for each variant) at 24°C. The protein buffer was 50 m*M* MES pH 6.8, 100 m*M* potassium chloride, 10% glycerol, 2 m*M* DTT. The D499N, W527H and S531E variant crystals grew as rectangular prisms within two days and reached full size within two weeks, whereas the GGG variant crystals grew as rectangular plates. Crystals were transferred into well solution supplemented with 15% (GGG variant), 20% (D499N variant) or 25% (W527H variant) ethylene glycol or 24% PEG 3350 and 20% ethylene glycol (S531E variant) as a cryoprotectant and flash-cooled in liquid nitrogen prior to data collection.

D499N variant crystals were grown using 3.6 mg ml$^{-1}$ purified protein pre-incubated with a final concentration of 10 m*M* pyruvate in a well solution consisting of 0.2 *M* ammonium citrate dibasic, 20% PEG 3350. W527H variant crystals were grown using 6.0 mg ml$^{-1}$ protein pre-incubated with a final concentration of 10 m*M* pyruvate in a well solution consisting of 0.325 *M* ammonium citrate dibasic, 16% PEG 3350. GGG variant crystals were grown using 2.0 mg ml$^{-1}$ protein in a well solution consisting of 0.2 *M* ammonium citrate pH 6.0, 24% PEG 3350. S531E variant crystals were grown using 2.0 mg ml$^{-1}$ protein in a well solution consisting of 0.2 *M* ammonium citrate pH 5.6, 16% PEG 3350. Crystallization information is summarized in Table 1.

### 2.4. Data collection and structure determination

Diffraction data were collected remotely using *Blu-Ice* (McPhillips *et al.*, 2002) on beamlines 12-2 (D499N variant) and 9-2 (W527H, GGG and S531E variants) at the Stanford Synchrotron Radiation Lightsource (SSRL), Menlo Park, California, USA. All data sets were collected at a wavelength of 0.97946 Å with 0.15° oscillation and 0.2 s exposure at a temperature of 100 K. For the D499N mutant, 110° of data were collected at a crystal-to-detector distance of 416 mm and were processed to 2.15 Å resolution in *XDS* (Kabsch, 2010). A phasing solution was determined by molecular replacement in *Phaser* (McCoy *et al.*, 2007) using the A and C domains of chain *A* of the S12D variant of hLPYK (PDB entry 4ip7; Holyoak *et al.*, 2013) as a rigid-body model, with a resulting log-likehood gain (LLG) of 21 178 and a translation-function *Z*-score (TFZ) of 18.6. For the W527H mutant, 180° of data were collected at a crystal-to-detector distance of 350 mm and were processed to 2.26 Å resolution in *autoPROC* (Vonrhein *et al.*, 2011) using an ellipsoidal resolution cutoff to account for the observed anisotropy. The ellipsoidal completeness in the outer shell exceeds 98% at 2.26 Å resolution. The spherical completeness in the outer shell exceeds 98% at 2.55 Å resolution. Following the PDB guidelines, we have deposited the merged intensities from *AIMLESS* (Evans & Murshudov, 2013) prior to resolution cutoff to allow unbiased reprocessing of the data for the W527H variant. Molecular replacement as described above resulted in an LLG of 17 337 and a TFZ of 66.6. For the GGG variant, which belonged to space group *P*1, 360° of data were collected at a crystal-to-detector distance of 385 mm and were processed to 2.32 Å resolution in *XDS*. The data set was 89.4% complete overall, but we have not been able to grow additional diffraction-quality GGG variant crystals in order to improve the data completeness. Molecular replacement resulted in an LLG of 30 905 and a TFZ of 88.0. For the S531E variant, 360° of data were collected at a crystal-to-detector distance of 430 mm and were processed to 2.42 Å resolution in *XDS*. Molecular replacement resulted in an LLG of 28 664 and a TFZ of 82.8.

For each structure, rounds of model building and refinement were completed in *Coot* (Emsley *et al.*, 2010) and *phenix.refine* (Adams *et al.*, 2010) and waters were placed by *phenix.refine*, corrected manually and verified using a $2mF_o - DF_c$ electron-density map contoured at $1.5\sigma$, following a round of refinement. For the D499N variant, density for Fru-1,6-BP in the allosteric site was visible following molecular replacement but was not modeled until after the polypeptide backbone had been refined. Statistics of data collection and refinement are listed in Tables 2 and 3.

### 2.5. Structure validation and model analysis

Summary data for the models, including residues and ligands built, are provided in Table 4. The PYK B domain

**Table 2**
Data collection and processing.

Values in parentheses are for the outer shell.

| Variant | D499N | W527H | GGG | S531E |
|---|---|---|---|---|
| Diffraction source | 12-2, SSRL | 9-2, SSRL | 9-2, SSRL | 9-2, SSRL |
| Wavelength (Å) | 0.97946 | 0.97946 | 0.97946 | 0.97946 |
| Temperature (K) | 100 | 100 | 100 | 100 |
| Detector | PILATUS 6M | PILATUS 6M | PILATUS 6M | PILATUS 6M |
| Crystal-to-detector distance (mm) | 416 | 350 | 385 | 430 |
| Rotation range per image (°) | 0.15 | 0.15 | 0.15 | 0.15 |
| Total rotation range (°) | 110 | 180 | 360 | 360 |
| Exposure time per image (s) | 0.2 | 0.2 | 0.2 | 0.2 |
| Space group | $P2_12_12$ | $P2_12_12$ | $P1$ | $P2_1$ |
| $a, b, c$ (Å) | 120.57, 204.66, 112.33 | 120.0, 204.6, 112.4 | 79.36, 106.21, 151.71 | 94.81, 139.22, 180.98 |
| $\alpha, \beta, \gamma$ (°) | 90, 90, 90 | 90, 90, 90 | 76.44, 80.06, 71.37 | 90, 103.34, 90 |
| Mosaicity (°) | 0.08 | 0.15 | 0.17 | 0.08 |
| Resolution range (Å) | 39.50–2.15 | 102.31–2.26 | 39.06–2.32 | 39.49–2.42 |
| Total No. of reflections | 628809 | 555901 | 684187 | 1210143 |
| No. of unique reflections | 150477 | 84688 | 175876 | 172562 |
| Completeness (%) | 99.0 (95.5) | 90.4 (98.8)† | 89.4 (76.9)‡ | 98.9 (92.1) |
| Multiplicity | 4.2 (4.2) | 6.6 (6.1) | 3.9 (3.4) | 7.0 (5.8) |
| $\langle I/\sigma(I)\rangle$ | 10.3 (2.0) | 14.9 (2.8) | 12.2 (2.0) | 16.4 (2.0) |
| $R_{\rm r.i.m.}$ (%) | 7.7 (64.6) | 9.3 (69.3) | 8.2 (65.6) | 8.9 (94.7) |
| Overall $B$ factor from Wilson plot (Å$^2$) | 34.47 | 29.92 | 38.45 | 45.68 |

† Processed using an ellipsoidal resolution cutoff to account for the observed anisotropy. The ellipsoidal completeness in the outer shell exceeds 98% at 2.26 Å. The spherical completeness in the inner shell exceeds 93% and that in outer shell exceeds 98% at 2.55 Å resolution. ‡ The completeness fell below 90% for this $P1$ crystal despite the collection of 360° of data. We were unable to collect additional data.

**Table 3**
Structure solution and refinement.

Values in parentheses are for the outer shell.

| Variant | D499N | W527H | GGG | S531E |
|---|---|---|---|---|
| Resolution range (Å) | 39.44–2.15 (2.20–2.15) | 54.18–2.26 (2.28–2.26) | 39.06–2.32 (2.38–2.32) | 39.54–2.42 (2.48–2.42) |
| Completeness (%) | 98.5 | 90.4 [ellipsoidal] | 89.4 | 98.7 |
| No. of reflections | | | | |
| Working set | 147251 (10216) | 84583 (1469) | 175816 (11360) | 173222 (11316) |
| Test set | 1982 (134) | 4187 (78) | 2000 (130) | 2006 (141) |
| Final $R_{\rm cryst}$ | 0.230 (0.3329) | 0.225 (0.256) | 0.191 (0.249) | 0.208 (0.267) |
| Final $R_{\rm free}$ | 0.253 (0.4128) | 0.264 (0.336) | 0.251 (0.305) | 0.260 (0.361) |
| No. of non-H atoms | | | | |
| Total | 13236 | 13016 | 29007 | 28375 |
| Protein | 12735 | 12811 | 28473 | 27957 |
| Ligand | 148 | 112 | 152 | 168 |
| Water | 353 | 195 | 382 | 250 |
| R.m.s. deviations | | | | |
| Bonds (Å) | 0.011 | 0.012 | 0.012 | 0.013 |
| Angles (°) | 1.142 | 1.268 | 1.252 | 1.318 |
| Average $B$ factors (Å$^2$) | | | | |
| Protein | 40.6 | 36.7 | 44.76 | 55.42 |
| Ramachandran plot | | | | |
| Most favored (%) | 97.13 | 98.05 | 96.65 | 95.23 |
| Allowed (%) | 2.5 | 1.64 | 2.97 | 3.88 |

(residues 130–230) interrupts the A domain. The B domain assumes multiple positions, forming limited contact with the A domain, and thus the resolution of the B domain is dependent on the crystal packing. The B domain was modeled only if the residues connecting it to the A domain were largely continuous, allowing accurate model building. As a result, unmodeled partial density exists for some of the B domains. The B domains were not modeled for the D499N and W527H variants, although broken density is present, contributing to higher $R_{\rm work}$ and $R_{\rm free}$ values for these structures. Geometry analysis was performed by *MolProbity* (Chen *et al.*, 2010). Thr340 in the active site is a consistent Ramachandran outlier that results from a hydrogen bond between the carbonyl O atom of Thr340 and the side chain of Arg306. Thr340 was also an outlier in the previously published hLPYK structures (Holyoak *et al.*, 2013) and has excellent density in each variant structure presented here. Rotameric outliers were found to comprise 2.4% (GGG variant), 1.5% (W527H variant), 1.43% (D499N variant) and 0.07% (S531E variant) of all residues.

Comparisons of structures and calculations of r.m.s.d. values were performed using *PDBeFold* (Krissinel & Henrick, 2004). Structure figures were generated in *PyMOL* v.2.0 (Schrödinger). The atomic coordinates and structure factors have been deposited in the Protein Data Bank with accession codes

**Table 4**
Model components.

| Protein | PDB code | ASU† | Ordered residues by chain | Waters | Ligands‡ |
|---|---|---|---|---|---|
| D499N | 6nn4 | 4 | *A*: 23–111, 117–130, 229–543<br>*B*: 24–110, 117–130, 231–543<br>*C*: 15–110, 117–130, 233–529, 532–543<br>*D*: 24–110, 117–133, 233–530, 532–543 | 353 | 4 Fru-1,6-BP, 4 phosphoenolpyruvate, 7 ethylene glycol |
| W527H | 6nn5 | 4 | *A*: 18–110, 117–129, 233–543<br>*B*: 23–110, 117–133, 232–543<br>*C*: 26–111, 116–129, 230–542<br>*D*: 23–111, 114–129, 229–543 | 195 | 10 ethylene glycol, 12 glycerol |
| GGG | 6nn7 | 8 | *A*: 16–137, 142–201, 205–527, 533–543<br>*B*: 26–132, 232–527, 533–543<br>*C*: 27–114, 117–543<br>*D*: 23–134, 142–148, 153–158, 163–176, 179–181, 186–195, 198–200, 211–224, 233–543<br>*E*: 25–543<br>*F*: 25–111, 116–131, 233–525, 534–543<br>*G*: 15–111, 117–135, 145–202, 205–213, 218–224, 233–527, 533–543<br>*H*: 27–110, 113–129, 234–490, 495–525, 534–542 | 382 | 2 citrate, 17 ethylene glycol, 14 glycerol |
| S531E | 6nn8 | 8 | *A*: 20–133, 144–155, 165–543<br>*B*: 23–138, 141–542<br>*C*: 18–135, 143–156, 166–200, 205–225, 233–543<br>*D*: 13–89, 92–129, 238–543<br>*E*: 23–137, 144–490, 494–529, 533–543<br>*F*: 22–110, 117–131, 230–529, 531–543<br>*G*: 20–89, 94–112, 116–130, 250–529, 533–543<br>*H*: 24–89, 92–110, 116–133, 236–243, 247–529, 53–543 | 250 | 42 ethylene glycol |

† Number of monomers in the asymmetric unit. ‡ Ethylene glycol was used as a cryoprotectant, citrate was in the well solution and glycerol was in the protein buffer.

6nn4 (D499N variant), 6nn5 (W527H variant), 6nn7 (GGG variant) and 6nn8 (S531E variant).

## 3. Results

Functional characterizations of all variants used in the current structural study have previously been reported (Ishwar *et al.*, 2015). X-ray diffraction data were collected to determine the crystal structures of the D499N, W527H, GGG and S531E variants of human liver pyruvate kinase in order to evaluate the structural determinants for allosteric loop motions in the presence and absence of Fru-1,6-BP. Each variant was generated by site-directed mutagenesis of the wild-type hLPYK sequence. The D499N, W527H and S531E variants are single-position substitutions that functionally mimic the activation (*i.e.* increased PEP affinity) caused by Fru-1,6-BP (Ishwar *et al.*, 2015). The GGG variant contains both a deletion of the proline at position 529 and a substitution of serine with glycine at position 531, thus shortening the allosteric loop by one residue. In the above structures, differences are only evident in the region surrounding the Fru-1,6-BP allosteric site and primarily involve the allosteric loop (residues 527–533).

### 3.1. Overall structure

The D499N and W527H variants crystallized in space group $P2_12_12$ with four monomers in the asymmetric unit arranged as a tetramer. The GGG and S531E variants crystallized in space groups $P1$ and $P2_1$, respectively, each with eight monomers, forming two tetramers, in the asymmetric unit. For the tetramers, the calculated surface areas for the interface between adjacent A domains (the A–A interface) range from 2502 to 2749 Å$^2$ and the interface surface areas between adjacent C domains (the C–C interface) range from 1421 to 1691 Å$^2$ across the four structures, as calculated by *PDBePISA* (Krissinel & Henrick, 2007). This is consistent with the previously published C436M (PDB entry 4ima) and S12D (PDB entry 4ip7) variants of hLPYK (Fig. 1, Supplementary Fig. S1). *PDBeFold* (Krissinel & Henrick, 2004) was used for comparisons of the overall structural homology. Alignments between structures were made for each combination of monomers of the variants presented here and of C436M (Supplementary Table S1). All structural alignments show high homology. The r.m.s.d. values ranged from 0.27 to 0.69 Å for the AC domains. For comparisons that included the B domains for the GGG (chains *A*, *C*, *D*, *E* and *G*) and S531E (chains *A*, *B*, *C* and *E*) variants, the r.m.s.d. values ranged as high as 2.23 Å. This was due to the varied conformations of the B domains. For example, the r.m.s.d. value of 2.23 Å is from a comparison between the GGG and C436M variants, in which the B domain of the GGG variant is rotated 26° relative to the B domain of the C436M variant according to *DynDom* (Girdlestone & Hayward, 2016). When the B domains are removed from the calculation, the r.m.s.d.s of the AC domain alignments decrease to below 0.6 Å. Alignments of the tetrameric form of each variant were performed by aligning C$^\alpha$ atoms across the A and C domains, but not the B domain (residue 130–230), using the combinatorial extension algorithm in *PyMOL*. These alignments also have low r.m.s.d. values ranging from 0.47 to 1.73 Å. The higher r.m.s.d. values (>1.0 Å) are found between variants that crystallize in different space groups (Supplementary Tables S1 and S2).

Thus, the structures of all of the generated variants share very similar global conformations, with the exception of the B domains, which are conformationally flexible except when stabilized by crystallographic contacts. This high homology leads us to conclude that the global structural changes that are likely to contribute to the allosteric mechanism are not represented in these structures, probably due to the low pH of the crystallization conditions (Fenton & Alontaga, 2009). Attempts were made to find a crystallization condition at a pH value above 7, but without success, and efforts are ongoing. Thus, we restrict our attention to the observed local changes in the allosteric loop within the allosteric site.

### 3.2. The allosteric site of the D499N variant

The structure of the D499N variant was determined in order to evaluate the structural basis of the recently proposed mechanism for the increased PEP affinity observed for the D499N variant. It was hypothesized that in the absence of Fru-1,6-BP Asp499 interacts across the C–C interface with Trp527′ and possibly with Arg528′ (Ishwar *et al.*, 2015). This hypothesis was supported by the $M_2$PYK structure (PDB entry 4fxj) in the absence of Fru-1,6-BP, in which Trp515 forms a 2.8 Å hydrogen bond to Asp487′ across the C–C interface (structurally equivalent to Trp527 and Asp499 in hLPYK; Morgan *et al.*, 2013). Thus, the D499N variant could prevent this interaction, such that the allosteric loop becomes less constrained in the absence of Fru-1,6-BP when compared with the wild-type protein.

The D499N variant was purified and crystallized in the absence of added Fru-1,6-BP; however, clear density corresponding to Fru-1,6-BP was visible in the allosteric sites of all four chains following molecular replacement. The position of Fru-1,6-BP matches that found in both the S12D and C436M variant structures (mutations that were included in previous structures in attempts to evaluate how the N-terminus of hLPYK interacts with the main body of the protein; Holyoak *et al.*, 2013) that were co-crystallized with added Fru-1,6-BP. The binding site is located between two loops: the phosphate-binding loop (residues 444–449) and the allosteric loop (residues 527–533). The 6′-phosphate of Fru-1,6-BP forms hydrogen bonds to the hydroxyl groups of Thr444, Thr446 and Ser449 from the phosphate-binding loop as well as to Ser531 from the allosteric loop. The 1′-phosphate forms an electrostatic interaction with Arg501. Finally, the C3, C4 and C5 hydroxyl groups of Fru-1,6-BP hydrogen-bond to the backbone amide and carbonyl groups of Arg528, Gly530 and Tyr533 in the allosteric loop (Fig. 2). To form these interactions, the allosteric loop must adopt a closed position to bring the residues into proximity to Fru-1,6-BP. In this position, the Tyr533, Arg528 and Trp527 side chains pack roughly parallel to each other and are directed out into solvent (Fig. 3*a*). We find that D499N is in a very similar position to Asp499 in the S12D and C436M structures. It is at distances of ∼13 Å from Arg528′ in the allosteric loop and 4.3 Å, on average, from Arg538 within the same subunit (Fig. 3*a*). Arg538 forms a cation–$\pi$ stacking interaction with the open form of the allosteric loop, as discussed below.

### 3.3. The allosteric site of the W527H variant

Similar to our reasoning for the D499N variant, the structure of the W527H variant was determined to examine the structural basis of the allosteric activation observed for the W527H variant (Ishwar *et al.*, 2015). The W527H variant was purified and crystallized in the absence of added Fru-1,6-BP. Weak density corresponding to solvent molecules such as glycerol and ethylene glycol was evident in the positions occupied by the 6′- and 1′-phosphates of Fru-1,6-BP in the structure of the D499N variant, but density suggesting bound Fru-1,6-BP was not evident. The D499N and W527H variants have a similar functional activity, making the presence of Fru-1,6-BP in the structure of the D499N variant and its absence in that of the W527H variant difficult to explain.

In the absence of Fru-1,6-BP (*i.e.* in the structure of the W527H variant), the position of the allosteric loop is quite different from that found in the structure of the D499N variant (Fig. 3*b*). Tyr533 is rotated 90° and packs parallel to Pro420. His527 is rotated 150° to form a cation–$\pi$ interaction across the C–C interface with Arg538 from the adjacent monomer. Residues 529–532 are not positioned to form hydrogen bonds to Fru-1,6-BP in this open conformation. With knowledge of the open conformation of the allosteric loop, we looked again at the structure of the D499N variant. Indeed, chain *C* of the structure of the D499N variant has weak density for the open allosteric loop, which is observed as the presence of density for Tyr533 parallel to Pro420 and of density for Tyr527 parallel to Arg538′. Because the structure of the D499N variant retains an unmodified allosteric loop, this suggests that the open position is sampled by the native loop and is not merely a result of the W527H mutation. Asp499 in the W527H variant is much closer to Arg538 and

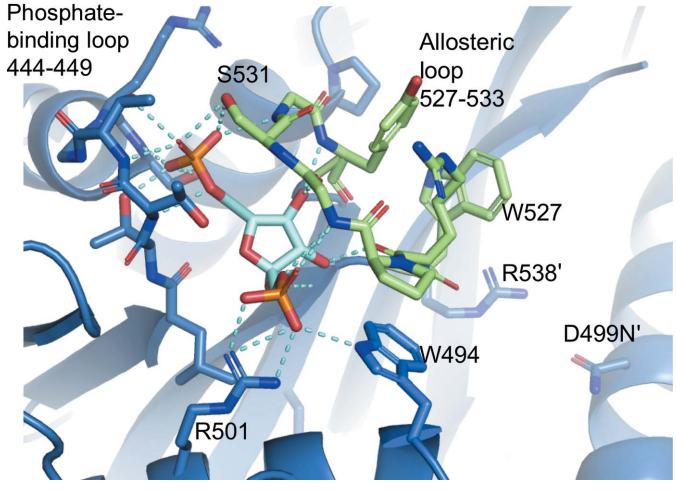


**Figure 2**
The allosteric site of the D499N variant. The allosteric loop is colored green. Fructose-1,6-bisphosphate is colored cyan. Arg538′ and D499N′ are located on the adjacent C domain across the C–C interface.

W527H′ (4.3 Å on average), but is still beyond hydrogen-bonding distance.

### 3.4. The allosteric site of the GGG variant

The GGG variant, with the deletion of Pro529 and an S531G substitution, is not activated by Fru-1,6-BP (Ishwar *et al.*, 2015). The original design of the GGG mutation was based on the idea that the shortened loop would not allow the formation of hydrogen bonds between the allosteric loop and Fru-1,6-BP. Fru-1,6-BP was not included in the crystallization condition and no Fru-1,6-BP was present in the allosteric site of the structure of the GGG variant. The allosteric loop adopts an open conformation that is fully resolved in three of the eight chains (Fig. 3*c*). Again, only solvent molecules, citrate or glycerol, could be modeled in the allosteric site and attempts at co-crystallization with Fru-1,6-BP did not yield diffracting crystals. In chains *C*, *D* and *E* Tyr533 opposes Pro420 and Trp527 stacks parallel to Arg538′, an interaction that is analogous to that seen in the structure of the W527H variant. Consistent with the original design of this variant, residues 530–532 of the GGG variant are held open and are not in a position to hydrogen-bond to Fru-1,6-BP. In the remaining chains the allosteric loop had incomplete electron density that could not be modeled.

### 3.5. The allosteric site of the S531E variant

The S531E variant has a higher affinity for PEP than wild-type hLPYK in the absence of Fru-1,6-BP (Ishwar *et al.*, 2015). The addition of Fru-1,6-BP causes only a very small additional increase in the affinity for PEP. Therefore, the S531E mutation serves as a mutational mimic of the allosteric activation caused by Fru-1,6-BP. It was hypothesized that the introduced negative charge of the glutamate in the S531E variant would bind in the position of the 6′-phosphate of Fru-1,6-BP (*i.e.* to the

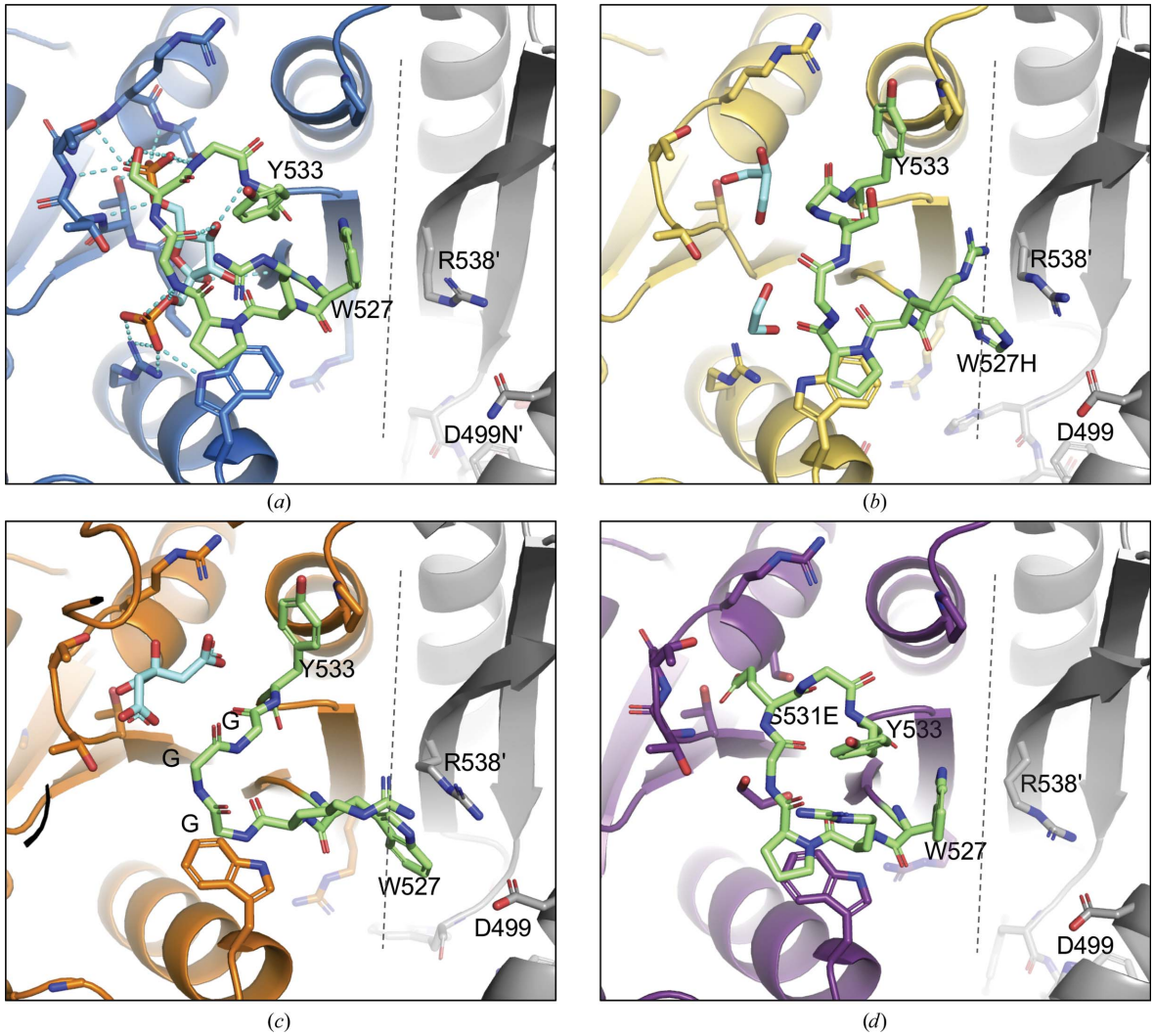


**Figure 3**
Comparison of the allosteric loop. The allosteric loop is colored green. Ligands are colored cyan. A dashed line marks the C–C interface. Adjacent monomers are colored gray. (*a*) The D499N variant. The D499N variant has a closed allosteric loop with fructose-1,6-bisphosphate (Fru-1,6-BP) bound. (*b*) The W527H variant. The allosteric loop is in an open position. W527H exhibits a cation–$\pi$ interaction with Arg538 across the C–C interface, stabilizing the conformation. (*c*) The GGG variant with an open allosteric loop. Trp527 forms a $\pi$-stacking interaction with Arg538. (*d*) The S531E variant with a closed allosteric loop. The Glu531 carboxylate is bound in the position of the 6′-phosphate of Fru-1,6-BP, stabilizing the closed conformation.

phosphate-binding 444–449 loop), thus stabilizing the allosteric loop in a closed position and leading to activation of the enzyme. The structure of the S531E variant, with eight chains, captures a variety of allosteric loop positions (closed, disordered and open; Supplementary Fig. S2). The allosteric loop is modeled in the closed position in five chains. In chain *C*, high-quality and complete electron density is present for the closed position, as seen in Fig. 3(*d*). In chain *B* the allosteric loop is modeled in the open position with partial occupancy. Density is incomplete for residues 530–532 in chains *E* and *G*. Overall, the density across the eight allosteric loops suggests a sampling of both open and closed conformations, with higher occupancy for the closed position. From the mosaic of conformations in the structure of the S531E variant, we conclude that the S531E variant is able to bind in the 6′-phosphate binding site; however, the loop is in flux, leading to partial allosteric activation, which is consistent with the previously collected kinetic data (Ishwar *et al.*, 2015).

## 4. Discussion

The crystal structures of hLPYK variants presented here have high global structural homology and appear to be in the same conformational state as those of the previously published C436M and S12D variants. Other pyruvate kinase enzymes, such as *Leishmania mexicana* PYK and human $M_2$PYK, have been shown to adopt alternative conformational states in the presence and absence of effector (Morgan *et al.*, 2010, 2013). We propose that the reason that the structures included in this study show local, but not global, changes is due to the pH of 6.0 and below in the crystallization drops for each of the variants. Allosteric coupling between PEP affinity and Fru-1,6-BP binding is known to decrease for hLPYK at low pH (Fenton & Alontaga, 2009; Fenton & Hutchinson, 2009). Thus, our structures may represent a fixed conformation that is determined primarily by pH and not by the presence or absence of effector.

Based on previous structural comparisons of $M_1$PYK and $M_2$PYK (Dombrauckas *et al.*, 2005; Morgan *et al.*, 2013) and outcomes from mutational studies of hLPYK, it was proposed that an interaction between Arg528 and Trp527 from one subunit and Asp499′ from the neighboring subunit was responsible for stabilizing the open form of the allosteric loop. Indeed, the D499N mutation and a series of substitutions at the 527 position all caused increased PEP affinity, even in the absence of Fru-1,6-BP (Ishwar *et al.*, 2015). The position of D499N is very similar to that of Asp499 in the structures of the S12D and C436M mutants (Supplementary Fig. S3). Due to the increased PEP affinity caused by the D499N position, we previously speculated that Asp499 interacts with Trp527′ and Arg538 in the wild-type protein, stabilizing the open allosteric loop, as homologous residues do in $M_2$PYK (Morgan *et al.*, 2013). However, this would require closing a distance of greater than 4 Å between Asp499 and W527H′ and Arg538. Again, it is possible that the low-pH crystallization conditions prevent conformational changes that would otherwise allow interaction between Asp499 and Trp527′. It is also possible that hLPYK undergoes far more subtle conformational changes to link effector binding to increased PEP affinity. Nevertheless, D499N does not appear to be in a position to interact with Trp527 or Arg528 and so the reason for the ability of D499N to mimic the allosteric effect of Fru-1,6-BP remains unresolved. Given that the Fru-1,6-BP must have originated from the cell and remained throughout purification, we suggest that Fru-1,6-BP binds tightly to the D499N variant. It is possible that the D499N variant protein included in the previous functional study also had Fru-1,6-BP present and that the presence of this activator caused the increased affinity for PEP.

These four hLPYK structures suggest that the allosteric loop toggles between a closed and an open position. In the absence of Fru-1,6-BP the loop is stabilized in the open position by interactions across the C–C interface between Arg538 and Trp527′. Once Fru-1,6-BP binds, the closed conformation is favored due to the hydrogen-bonding network between the allosteric loop and Fru-1,6-BP. Of the changes in the allosteric loop, Tyr533 and Trp527 undergo the most significant repositioning. In the closed form, with Fru-1,6-BP bound, Tyr533 and Trp527 pack proximal to each other and are exposed to solvent. In the open form, Tyr533 packs parallel to Pro420 and W527H forms a cation–$\pi$ interaction with Arg538′ across the C–C interface. Further structural studies will be necessary to determine how conformational changes of the allosteric loop of hLPYK lead to altered PEP affinity in the active site.

## Acknowledgements

Use of the Stanford Synchrotron Radiation Lightsource, SLAC National Accelerator Laboratory is supported by the US Department of Energy, Office of Science, Office of Basic Energy Sciences under Contract DE-AC02-76SF00515. The Stanford Synchrotron Radiation Lightsource Structural Molecular Biology Program is supported by the US Department of Energy Office of Biological and Environmental Research and by NIGMS, NIH Grant P41GM103393. The authors declare that they have no conflicts of interest with the contents of this article. The content is solely the responsibility of the authors and does not necessarily represent the official views of the NIH. We thank Lauren Arney and Azel King for their work on PYK variant purification trials.

## Funding information

This work was supported by NIH Grant GM115340 to AWF, NIH Grant GM127655 to ALL and NSF Grant CHE1403293 to ALL. JSM and TAR were supported by the NIH Graduate Training Program in the Dynamic Aspects of Chemical Biology Grant T32 GM008545 and JSM was supported by an American Heart Association Predoctoral Fellowship PRE33960374.

## References

Adams, P. D., Afonine, P. V., Bunkóczi, G., Chen, V. B., Davis, I. W., Echols, N., Headd, J. J., Hung, L.-W., Kapral, G. J., Grosse-

Kunstleve, R. W., McCoy, A. J., Moriarty, N. W., Oeffner, R., Read, R. J., Richardson, D. C., Richardson, J. S., Terwilliger, T. C. & Zwart, P. H. (2010). *Acta Cryst.* D**66**, 213–221.
Carlson, G. M. & Fenton, A. W. (2016). *Biophys. J.* **110**, 1912–1923.
Chen, V. B., Arendall, W. B., Headd, J. J., Keedy, D. A., Immormino, R. M., Kapral, G. J., Murray, L. W., Richardson, J. S. & Richardson, D. C. (2010). *Acta Cryst.* D**66**, 12–21.
Dombrauckas, J. D., Santarsiero, B. D. & Mesecar, A. D. (2005). *Biochemistry*, **44**, 9417–9429.
Emsley, P., Lohkamp, B., Scott, W. G. & Cowtan, K. (2010). *Acta Cryst.* D**66**, 486–501.
Evans, P. R. & Murshudov, G. N. (2013). *Acta Cryst.* D**69**, 1204–1214.
Fenton, A. W. & Alontaga, A. Y. (2009). *Methods Enzymol.* **466**, 83–107.
Fenton, A. W. & Hutchinson, M. (2009). *Arch Biochem Biophys.* **484**, 16–23.
Girdlestone, C. & Hayward, S. (2016). *J. Comput. Biol.* **23**, 21–26.
Holyoak, T., Zhang, B., Deng, J., Tang, Q., Prasannan, C. B. & Fenton, A. W. (2013). *Biochemistry*, **52**, 466–476.
Ishwar, A., Tang, Q. & Fenton, A. W. (2015). *Biochemistry*, **54**, 1516–1524.
Jurica, M. S., Mesecar, A., Heath, P. J., Shi, W., Nowak, T. & Stoddard, B. L. (1998). *Structure*, **6**, 195–210.
Kabsch, W. (2010). *Acta Cryst.* D**66**, 125–132.
Krissinel, E. & Henrick, K. (2004). *Acta Cryst.* D**60**, 2256–2268.
Krissinel, E. & Henrick, K. (2007). *J. Mol. Biol.* **372**, 774–797.
McCoy, A. J., Grosse-Kunstleve, R. W., Adams, P. D., Winn, M. D., Storoni, L. C. & Read, R. J. (2007). *J. Appl. Cryst.* **40**, 658–674.
McPhillips, T. M., McPhillips, S. E., Chiu, H.-J., Cohen, A. E., Deacon, A. M., Ellis, P. J., Garman, E., Gonzalez, A., Sauter, N. K., Phizackerley, R. P., Soltis, S. M. & Kuhn, P. (2002). *J. Synchrotron Rad.* **9**, 401–406.
Morgan, H. P., McNae, I. W., Nowicki, M. W., Hannaert, V., Michels, P. A., Fothergill-Gilmore, L. A. & Walkinshaw, M. D. (2010). *J. Biol. Chem.* **285**, 12892–12898.
Morgan, H. P., O'Reilly, F. J., Wear, M. A., O'Neill, J. R., Fothergill-Gilmore, L. A., Hupp, T. & Walkinshaw, M. D. (2013). *Proc. Natl Acad. Sci. USA*, **110**, 5881–5886.
Valentini, G., Chiarelli, L. R., Fortin, R., Dolzan, M., Galizzi, A., Abraham, D. J., Wang, C., Bianchi, P., Zanella, A. & Mattevi, A. (2002). *J. Biol. Chem.* **277**, 23807–23814.
Vonrhein, C., Flensburg, C., Keller, P., Sharff, A., Smart, O., Paciorek, W., Womack, T. & Bricogne, G. (2011). *Acta Cryst.* D**67**, 293–302.